Manifold learning characterization of abnormal myocardial motion patterns: application to CRT-induced changes

Nicolas Duchateau, Gemma Piella, Adelina Doltra, Lluis Mont, Josep Brugada, Marta Sitges, Bart Bijnens, Mathieu de Craene

Manifold learning characterization of abnormal myocardial motion patterns: application to CRT-induced changes.

Nicolas Duchateau[1], Gemma Piella[2], Adelina Doltra[1], Lluis Mont[1], Josep Brugada[1], Marta Sitges[1], Bart Bijnens[2,3], and Mathieu De Craene[4]

[1] Hospital Clínic - IDIBAPS - Universitat de Barcelona, Spain
[2] Universitat Pompeu Fabra, Barcelona, Spain
[3] ICREA, Barcelona, Spain
[4] Philips Research, Medisys, Suresnes, France

Abstract. The present paper aims at quantifying the evolution of a given motion pattern under cardiac resynchronization therapy (CRT). It builds upon techniques for population-based cardiac motion quantification (statistical atlases, for inter-sequence spatiotemporal alignment and the definition of normal/abnormal motion). Manifold learning is used on spatiotemporal maps of myocardial motion abnormalities to represent a given abnormal pattern and to compare any individual to that pattern. The methodology was applied to 2D echocardiographic sequences in a 4-chamber view from 108 subjects (21 healthy volunteers and 87 CRT candidates) at baseline, with pacing ON, and at 12 months follow-up. Experiments confirmed that recovery of a normal motion pattern is a necessary but not sufficient condition for CRT response.

1 Introduction

Mechanisms-based characterization of motion and deformation has recently shown its potential to improve our understanding of the etiologies of heart failure [2]. In the context of cardiac resynchronization therapy (CRT), where the important rate of non-response still needs to be reduced [3], mechanical dyssynchrony is recommended to be assessed before and after treatment. However, due to the complexity of the observable patterns, single measurements of mechanical dyssynchrony (in particular, time-to-event and peak magnitude measurements) rapidly showed strong limitations [8]. For a more comprehensive analysis, recently published studies recommend to first identify potential sources of dyssynchrony by looking at specific motion and deformation patterns. This can be achieved through visual inspection or pattern-specific measurements [13] [11].

Learning the representations of such patterns is mostly done visually by each clinician as part of his/her clinical routine. Furthermore, current quantification tools are not targeted towards intra- and inter-subject comparison of patterns. Main limitations hampering this are the lack of (i) a common spatiotemporal reference system to compare subjects, and of (ii) efficient pattern analysis tools

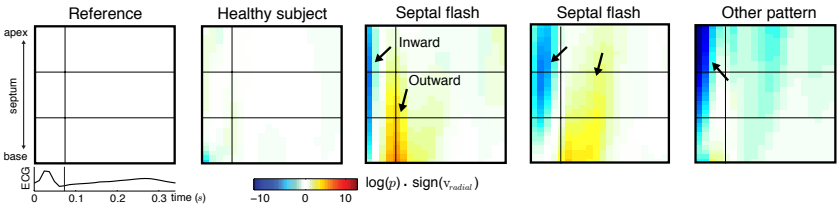

Fig. 1: 2D maps of spatiotemporal motion abnormalities used as input for the method presented in this paper. A variety of the patterns that may be observed.

to actually compare patterns and not only information at each voxel or segment separately. The first point has been addressed by methods derived from computational anatomy (an overview of recent advances is given in [12]), providing both an anatomical reference and a framework to transport subject-specific information to this reference. The second point may be addressed by the use of dimensionality reduction techniques to describe the principal characteristics of the studied patterns. One of the main issues here is whether the inter-subject variability (and therefore, the studied pattern) can be accurately described by linear or non-linear techniques (a selected review is done in [1]).

In the present paper, we are interested in characterizing the motion patterns of a population of CRT candidates from 2D echocardiographic sequences before and after the therapy (baseline, with pacing ON, and at follow-up). We build upon recent methods for the spatiotemporal alignment of motion information (myocardial velocities) to a common reference and population-wise characterization of normality (statistical atlas of motion [5]). This allows local quantification of abnormal motion and qualitative observations of the variety of abnormal motion patterns in CRT candidates, in relation to CRT response [7]. However, these methods still do not reach a quantification (of CRT-induced changes) based on pattern comparison. In the present paper, we use a recent method representing a specific abnormal motion patterns as a pathological deviation from normality [6]. We extend this analysis to a pattern-wise understanding of CRT-induced changes in myocardial motion and their relation with CRT response.

2 Methods

2.1 Learning the pattern representation as manifold

Manifold learning is first used on a population with a specific abnormal motion pattern, assuming that this pattern can be represented by a (non-linear) manifold. Maps of motion abnormalities [5], representing patterns of (ab)normal motion (Fig.1), are used as input images for our method. However, our algorithm is independent of the input image type, provided the above-mentioned hypothesis holds. For this reason, we kept the formulation general in this section. Application-oriented details and interpretation are given further.

All the images considered in this paper belong to an ambient space $\mathcal{A} \subset \mathbb{R}^P$, where P is the number of pixels in each image, and are compared according to

the metric $S_{\mathcal{A}} : \mathcal{A} \times \mathcal{A} \to \mathbb{R}^+$. The subgroup of $N+1$ images used for learning the manifold $\mathcal{M} \subset A$ is denoted $\mathcal{I} = \{\mathbf{I}_0, ..., \mathbf{I}_N\} \subset \mathcal{A}$.

Learning is performed through the isomap algorithm [14], which provides a set of coordinates $\mathcal{X} = \{\mathbf{x}_0, ..., \mathbf{x}_N\} \subset \mathcal{C}$, where $\mathcal{C} \subset \mathbb{R}^M$ is the coordinate space of the surface defining the manifold, of estimated dimensionality M, and equipped with the metric $S_{\mathcal{C}} : \mathcal{C} \times \mathcal{C} \to \mathbb{R}^+$.

2.2 Mapping new subjects

Any image $\mathbf{I} \in \mathcal{A}$ is then associated to another image in the manifold $\hat{\mathbf{I}} \in \mathcal{M}$, using the composition of the correspondence functions $f : \mathcal{A} \to \mathcal{C}$ and $g : \mathcal{C} \to \mathcal{A}$,

$$\hat{\mathbf{I}} = g \circ f(\mathbf{I}). \tag{1}$$

In the following, we assume that the manifold may not pass exactly by the training set ($\mathcal{I} \not\subset \mathcal{M}$) for all but one image, used as origin, by convention chosen to be $\mathbf{I}_0$. In the specific context of our application, where images correspond to 2D maps of abnormality, the origin $\mathbf{I}_0$ corresponds to a synthetic image representing a perfectly normal motion pattern (0 value at every pixel, Sec.3.2), and is added to the real dataset $\{\mathbf{I}_1, ..., \mathbf{I}_N\}$ before any computation.

f and g can be estimated using interpolation techniques, inspired from the concept of principal curves [10]. Under the assumption that $\mathcal{I} \not\subset \mathcal{M}$, this can be formulated as an inexact matching problem, adapted to force the interpolation function to pass by the origin coordinates $\mathbf{x}_0$ or image $\mathbf{I}_0$ (in the case of f or g, respectively). For the sake of clarity, we detail the formulations for f only, similar expressions being obtained for g by interchanging the role of images and coordinates. Using the framework of reproducible kernel Hilbert spaces (RKHS, see [6] for further details on the present application), this leads to set:

$$f(\mathbf{I}) = \sum_{i=0}^{N} k_{\mathcal{F}}(\mathbf{I}, \mathbf{I}_i) \cdot \mathbf{c}_i \quad \text{with} \quad \mathbf{C} = \Big(\mathbf{K}_{\mathcal{I}} + \frac{1}{\gamma_f}\mathbf{M}\Big)^{-1} \cdot \mathbf{X}, \tag{2}$$

where γ_f is a weighting coefficient balancing the smoothness of the interpolation and the adherence to the data, $\mathbf{C} = (\mathbf{c}_0, \ldots, \mathbf{c}_N)^t$ and $\mathbf{X} = (\mathbf{x}_0, \ldots, \mathbf{x}_N)^t$ both $\in \mathbb{M}_{N+1,M}$ (the set of $(N+1) \times M$-dimensional real-valued matrices), and $\mathbf{K}_{\mathcal{I}} = \big(k_{\mathcal{F}}(\mathbf{I}_i, \mathbf{I}_j)\big)_{(i,j)\in[0,N]^2}$ and $\mathbf{M} = \big(M_{i,j}\big)_{(i,j)\in[0,N]^2}$ both $\in \mathbb{M}_{N+1,N+1}$, with $M_{i,i} = 1\ \forall i \neq 0$ and 0 otherwise. The scalar function $k_{\mathcal{F}}$ defining the kernel $K_{\mathcal{F}}$ is chosen as $k_{\mathcal{F}}(\mathbf{I}, \mathbf{J}) = \exp\big(-S_{\mathcal{A}}(\mathbf{I}, \mathbf{J})^2/\sigma_{\mathcal{F}}^2\big)$, with $(\mathbf{I}, \mathbf{J}) \in \mathcal{A}^2$, $\sigma_{\mathcal{F}}$ being its bandwidth.

2.3 Distance computation and statistical analysis

The composition of f and g (Eq.1) allows defining two distances $\mathcal{A} \to \mathbb{R}^+$: d_P, between any image $\mathbf{I} \in \mathcal{A}$ and the manifold [9], and d_M, which compares individuals to the origin along the manifold structure:

$$d_P(\mathbf{I}) = S_{\mathcal{A}}(\hat{\mathbf{I}}, \mathbf{I}) \quad \text{and} \quad d_M(\mathbf{I}) = S_{\mathcal{C}}\big(f(\mathbf{I}), \mathbf{x}_0\big). \tag{3}$$

These two distances provide a 2D space into which any image $\mathbf{I} \in \mathcal{A}$ is mapped. In the case of our application (Sec.3), each image corresponds to (the motion abnormalities of) one subject at a given stage of the therapy. The visualization of individual data in this 2D space was complemented by groupwise statistical comparisons of 2D unpaired and paired data. Fisher's linear discriminant was used to find the direction of maximum separation between each pair of compared groups, and 1D statistical tests were performed along this direction: Mann-Whitney U-test (inter-group comparison), and Wilcoxon signed-rank test (paired data). Non-parametric tests were preferred due to the limited number of samples in each class. p-values below 0.05 were considered as statistically significant difference between the tested groups. All data were analyzed using the SPSS statistical package v.15.0 (SPSS Inc., Chicago, IL).

3 Experiments and results

3.1 Dataset description

The method was applied to a database of 108 subjects (21 healthy volunteers and 87 CRT candidates acquired at baseline, with CRT pacing ON, and at 12 months paced follow-up). 56 patients shared a specific abnormal motion pattern of intra-ventricular dyssynchrony at baseline, also referred to as septal flash (SF) or septal rebound stretch [13] [11]. This pattern is highly related to the presence of left bundle branch block and has been shown to highly determine CRT response, although the link between this electrical dyssynchrony and its mechanical manifestations has not been fully established yet. It is characterized by a fast inward/outward motion of the septum during the isovolumic contraction, and is visible on radial displacement and velocity traces. 2D echocardiographic sequences were acquired for these subjects in a 4-chamber view, in which the septum is fully visible from base to apex, with a temporal resolution high enough to accurately characterize fast patterns such as a SF (around 60 fps for the volunteers and 30 fps for the CRT candidates, who have dilated hearts and therefore require the use of a broader ultrasound sector, resulting in a lower frame rate).

Clinical characteristics about the groups of volunteers and CRT candidates were detailed in [7]. From a statistical point-of-view, additional justifications about the use of such a population were extensively described in [5].

3.2 Input images: 2D spatiotemporal maps of motion abnormalities

Motion (myocardial velocities) was estimated along these sequences using temporal diffeomorphic free-form deformation (TDFFD [4]), which enforces temporal consistency and provides differentiable velocities. These velocities were spatiotemporally aligned to a common reference using the framework of [5], and the 2D spatiotemporal abnormality maps were computed (Fig.1). In these maps, the horizontal and vertical axes are time (systole only) and space (position along the septum, from base to apex), respectively. Each pixel of a given map corresponds

	N		d_M	d_P	p vs. BAS	p vs. Healthy
Healthy	19	BAS	16.5 ± 9.3	21.3 ± 15.8	.	.
		BAS	60.6 ± 27.5	10.1 ± 5.5	.	< 0.001
SF (training + tested)	56	ON	32.4 ± 19.9	32.5 ± 15.6	< 0.001	0.002
		FU	33.5 ± 17.3	34.0 ± 16.6	< 0.001	< 0.001
		BAS	32.1 ± 17.9	26.4 ± 14.2	.	0.037
Other	31	ON	36.2 ± 27.7	32.2 ± 12.7	0.014	0.012
		FU	28.2 ± 15.2	41.6 ± 30.0	0.002	0.006

Table 1: Average values of d_P and d_M for each subpopulation at baseline (BAS), with pacing ON, and follow-up (FU).

to a statistical index computed at this spatiotemporal location to estimate abnormality (p-value resulting from the Mahalanobis distance when comparing the studied subject to the healthy population of 21 healthy volunteers; in the present application, the logarithm of this p-value is used to get better readability of the abnormality scale, and multiplied by the sign of the radial velocity to differentiate between inward and outward motion of the septum [5]). According to these conventions, the origin image $\mathbf{I}_0$ (Sec.2.2) is defined as an image having 0 value at every pixel, which therefore corresponds to a perfectly normal motion pattern.

3.3 Parameters optimization

Optimal values for the method parameters were previously estimated for this dataset [6], and are only listed here due to text extent constraints. Training was done on a subgroup of 50 SF patients. Dimensionality and number of K-NN were estimated to be $M = 4$ and $K = 5$. Kernels bandwidths were locally adapted depending on the neighborhood size to prevent from non-uniformities in the points distribution, and set to the average distance between the K-NN [6]. The weighting terms were found to be $\log(\gamma_f) = 1$ and $\log(\gamma_g) = 0.5$.

3.4 Pattern-based analysis of CRT induced-changes

The analysis was performed in the 2D space defined by d_P and d_M (interpretable here as distance to the SF pattern, and distance to normality along the estimated manifold, respectively). Normality range was defined relatively to the covariance computed for the healthy population (19 healthy volunteers; two of them were considered as outliers due to high velocities [and therefore higher abnormality values], but normal velocity patterns). It corresponded to the ellipse of semi-minor/major axes twice bigger than the one obtained from PCA on this subpopulation (in this 2D space). This value was used as threshold to label patients who (at follow-up) recovered a normal motion pattern and the ones remaining abnormal.

Analysis per population Fig.2a represents the 2D space formed by d_P and d_M including all subjects. At baseline, patients with SF have low d_P (both

	N		d_M	d_P	p vs. BAS	p vs. Healthy
Resp., recov.	22	BAS	65.8 ± 29.6	11.6 ± 6.0	.	< 0.001
		ON	32.8 ± 20.4	34.0 ± 18.7	< 0.001	0.008
		FU	19.5 ± 7.7	26.7 ± 9.6	< 0.001	NS
Resp., non-recov.	21	BAS	54.4 ± 23.5	8.6 ± 5.0	.	< 0.001
		ON	26.3 ± 14.9	31.4 ± 13.2	0.005	< 0.001
		FU	48.0 ± 15.1	33.7 ± 16.7	0.002	0.001
Non-resp.	12	BAS	61.0 ± 31.1	10.5 ± 5.3	.	< 0.001
		ON	43.5 ± 25.2	27.8 ± 7.8	< 0.001	NS
		FU	33.9 ± 11.9	48.0 ± 18.8	< 0.001	< 0.001

Table 2: Average values of d_P and d_M for each subgroup of SF patients at baseline (BAS), with pacing ON, and follow-up (FU). NS: non-significant p-value.

training set and tested subjects; the value of d_P for the training ones reflects the adherence to the data retained in the inexact matching problem). Their arrangement according to d_M actually corresponds to the amount of abnormality observed in each map, when looked at individually. Patients with an abnormal pattern different from SF are farther from the manifold (higher d_P) and out of the normality range. The limits of more conventional approaches to perform the same analysis were discussed in detail in [6], including concrete comparisons with the linear case (PCA).

Under the effect of pacing (both CRT ON and follow-up), patients with SF at baseline reach higher values of d_P, reflecting that the SF pattern tends to disappear, and lower values of d_M, meaning either that they get closer to normality, or that their new motion pattern cannot be accurately reconstructed from the training population. However, the first hypothesis can be confirmed from a direct look at echocardiographic sequences. Patients without SF at baseline tend to reduce abnormalities, and the observed pattern does not turn into a SF. Statistical analysis of these values is given in Tab.1 as complement.

Link with CRT response (SF only) Fig.2b relates the previous analysis with CRT response (defined as a reduction $\geq 15\%$ in left-ventricular end-systolic volume, without heart transplantation). This analysis is performed for the subset of SF patients only. Indeed, for the patients without SF at baseline (with another abnormal pattern), our method is only able to tell if the pattern got closer to SF/normality, but not if this abnormal pattern is still present or not (as the manifold is learnt from a subgroup of SF patients only). Patients are divided into responders who recovered a normal motion at follow-up (who went within the normality range defined by the healthy population covariance), responders for which abnormal motion is still present (out of this range), and non-responders. At baseline, no difference is visible between these subgroups, meaning that the presence of SF is not a sufficient condition for CRT response. In these subgroups, the SF pattern tends to disappear with pacing ON (higher d_P) and motion gets closer to normality (lower d_M), but the three groups are still mixed. On

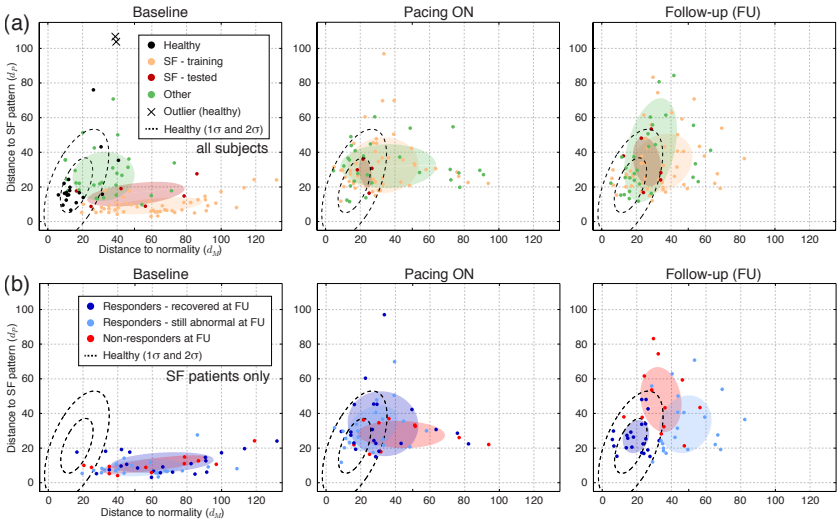

Fig. 2: 2D representation of the studied subjects (according to d_P and d_M) at baseline, with pacing ON, and follow-up (FU). (a) all subjects; (b) SF patients only.

the contrary, larger inter-group separation is observed at follow-up. Patients who recovered normal motion are within the range of healthy volunteers (by definition), and are almost all responders. Patients with abnormal motion still present may eventually be responders or not. This confirms that the recovery of a normal motion pattern is a necessary but not sufficient condition for CRT response. Statistical analysis of these values is given in Tab.2 as complement.

Limitations Note that our objective is not to achieve perfect clustering between the different subgroups. Our method compares individuals to the manifold learnt for SF only, meaning that clustering between the other classes may not be achieved. The tolerance to the data dispersion around the learnt manifold may also lower the clustering ability, when comparing individuals to the SF pattern.

One should remember that the overall evolution of individuals with CRT is probably more complex than uniquely motion-based observations. The correction of motion abnormalities is one characteristic to look at, among others such as clinical condition and remodeling. However, the population analysis presented here already allows to understand part of the overall evolution of the considered subpopulations, and the statistical tests used (dealing with groups means and distribution) served for adding a quantitative index to this evolution.

4 Conclusion

We presented a method for the comparison of myocardial motion patterns, including a way to represent a given abnormal pattern as a deviation from nor-

mality. In the context of CRT, the interest of our method resides in performing population-wise analysis of relevant patterns and quantifying therapy-induced changes of these patterns, which may overcome the limitations of current quantitative studies. Additionally, this approach allows to identify patients that have a non-typical behavior (e.g. responders with still abnormal motion). Investigating this further on from a clinical point-of-view might open up new directions towards understanding cardiovascular diseases.

Acknowledgements. This work was supported by the Spanish Industrial and Technological Development Center (cvREMOD CEN-20091044). The authors acknowledge their collaborators on the previous steps this work is based on (E Silva, MA Castel, Hospital Clínic, Barcelona, ES; AF Frangi, University of Sheffield, UK).

References

1. J Ashburner and S Klöppel. Multivariate models of inter-subject anatomical variability. *Neuroimage*, 56:422–39, 2011.
2. BH Bijnens, M Cikes, C Butakoff, et al. Myocardial motion and deformation: What does it tell us and how does it relate to function? *Fetal Diagn Ther*, 32:5–16, 2012.
3. GB Bleeker, JJ Bax, JWH Fung, et al. Clinical versus echocardiographic parameters to assess response to cardiac resynchronization therapy. *Am J Cardiol*, 97:260–3, 2006.
4. M De Craene, G Piella, O Camara, et al. Spatiotemporal diffeomorphic free-form deformation: Application to motion and strain estimation from 3D echocardiography. *Med Image Anal*, 16:427–50, 2012.
5. N Duchateau, M De Craene, G Piella, et al. A spatiotemporal statistical atlas of motion for the quantification of abnormalities in myocardial tissue velocities. *Med Image Anal*, 15:316–28, 2011.
6. N Duchateau, M De Craene, G Piella, et al. Constrained manifold learning for the characterization of pathological deviations from normality. *Med Image Anal*, 16:1532–49, 2012.
7. N Duchateau, A Doltra, E Silva, et al. Atlas-based quantification of myocardial motion abnormalities: added-value for understanding the effect of cardiac resynchronization therapy. *Ultrasound Med Biol*, 38:2186–97, 2012.
8. BK Fornwalt. The dyssynchrony in predicting response to cardiac resynchronization therapy: a call for change. *J Am Soc Echocardiogr*, 24:180–4, 2011.
9. S Gerber, T Tasdizen, PT Fletcher, et al. Manifold modeling for brain population analysis. *Med Image Anal*, 14:643–53, 2010.
10. T Hastie and W Stuetzle. Principal curves. *J Am Stat Assoc*, 84:502–16, 1989.
11. J Lumens, GE Leenders, MJ Cramer, et al. Mechanistic evaluation of echocardiographic dyssynchrony indices: patient data combined with multiscale computer simulations. *Circ Cardiovasc Imaging*, 5:491–9, 2012.
12. MI Miller and A Qiu. The emerging discipline of computational functional anatomy. *Neuroimage*, 45:S16–39, 2009.
13. C Parsai, BH Bijnens, GR Sutherland, et al. Toward understanding response to cardiac resynchronization therapy: left ventricular dyssynchrony is only one of multiple mechanisms. *Eur Heart J*, 30:940–9, 2009.
14. JB Tenenbaum, V De Silva, and JC Langford. A global geometric framework for nonlinear dimensionality reduction. *Science*, 290:2319–23, 2000.